

1 **Foxp3 Orchestrates Reorganization of Chromatin Architecture to Establish**
2 **Regulatory T Cell Identity**

3

4 Zhi Liu^{1,2,#}, Dong-Sung Lee^{3,4,#}, Yuqiong Liang¹, Ye Zheng^{1,*}, and Jesse R Dixon^{3,*}

5

6 1. NOMIS Center for Immunobiology and Microbial Pathogenesis, Salk Institute for
7 Biological Studies, La Jolla, CA, USA

8 2. Shanghai Immune Therapy Institute, Renji Hospital, Shanghai Jiao Tong University
9 School of Medicine, Shanghai, China

10 3. Gene Expression Laboratory, Salk Institute for Biological Studies, La Jolla, CA, USA

11 4. Department of Life Sciences, University of Seoul, Seoul, South Korea

12

13 # Co-first authors

14 * Co-corresponding authors

15

16

17

18 **SUMMARY**

19 **Chromatin conformation reorganization is emerging as an important layer of**
20 **regulation for gene expression and lineage specification. Yet, how lineage-specific**
21 **transcription factors contribute to the establishment of cell type-specific 3D**
22 **chromatin architecture in the immune cells remains unclear, especially for the late**
23 **stages of T cell subset differentiation and maturation. Regulatory T cells (Treg) are**
24 **mainly generated in the thymus as a subpopulation of T cells specializing in**
25 **suppressing excessive immune responses. Here, by comprehensively mapping 3D**
26 **chromatin organization during Treg cell differentiation, we show that Treg-specific**
27 **chromatin structures were progressively established during its lineage**
28 **specification, and highly associated with Treg signature gene expression.**
29 **Additionally, the binding sites of Foxp3, a Treg lineage specifying transcription**
30 **factor, were highly enriched at Treg-specific chromatin loop anchors. Further**
31 **comparison of the chromatin interactions between wide-type Tregs versus Treg**
32 **cells from Foxp3 knock-in/knockout or newly-generated Foxp3 domain-swap**
33 **mutant mouse revealed that Foxp3 was essential for the establishment of Treg-**
34 **specific 3D chromatin architecture, although it was not dependent on the formation**
35 **of the Foxp3 domain-swapped dimer. These results highlighted an**
36 **underappreciated role of Foxp3 in modulating Treg-specific 3D chromatin structure**
37 **formation.**

38

39 INTRODUCTION

40 Genome-wide 3D chromosome conformation capture technologies have revealed
41 that higher-order 3D chromatin structures of mammalian genome are hierarchically
42 organized into chromosome territories, A/B compartments, topologically associating
43 domains (TADs), and chromatin loops¹⁻⁵. TADs are genomic regions that self-interact but
44 insulate regions outside the domain, therefore contributing to the regulation of gene
45 expression by restricting interactions of cis-regulatory elements to their target genes⁶⁻⁸.
46 Zinc-finger transcription factor CTCF and the ring-shaped cohesin complex play critical
47 roles in the formation and maintenance of TADs across different cell lineages⁹. However,
48 these ubiquitously expressed proteins alone cannot establish and maintain cell lineage-
49 specific genome architecture. Lineage-specific transcription factors have been proposed
50 to regulate genome organization in specific cell lineages^{8,10,11}. As for T cells in the immune
51 system, it has been revealed that Bcl11b and TCF1 controls 3D chromatin architectures
52 during early T cell development¹²⁻¹⁴. However, little is known about global genome
53 organization for the late stage of T cell development and differentiation.

54 Regulatory T cells (Treg) are a subset of CD4+ T cells subset that suppress
55 excessive immune responses. Treg cell lineage specification represents one of the final
56 stages of T cell development and thus is an excellent model to examine the roles of
57 lineage-specific transcription factors in 3D genome organization^{15,16}. Foxp3, an X
58 chromosome-encoded gene in the forkhead transcription factor family, plays a central role
59 in Treg cell lineage specification, phenotypic stability, metabolic fitness, and regulatory
60 function¹⁷⁻²⁴. Depending on the activating or repressing cofactors it associates with^{21,25},
61 Foxp3 can either promote or inhibit target gene expression by exploiting pre-existing

62 enhancer landscapes²⁶. A recent study using HiChIP showed that Foxp3 was associated
63 with enhancer-promoter loops to fine tune Foxp3-dependent gene expression²⁷. However,
64 it remains elusive how the Treg 3D chromatin architecture is established during their
65 lineage specification, how it influences gene expression in Tregs, and whether and how
66 Foxp3 contributes to Treg-specific chromatin interactions. Considering it was reported
67 that Foxp3 has the capability to bring two distal DNA elements together through the
68 formation a domain-swapped dimer²⁸, it would be of great interest to test whether that
69 Foxp3 can function as a loop anchor protein to directly contribute to the establishment of
70 Treg-specific TADs and chromatin loops.

71 Here, we comprehensively mapped the chromatin interactions across different
72 Treg developmental stages in the thymus, and Treg and Tcon cells in the spleen by in
73 situ Hi-C. Our findings revealed that the 3D genome of Treg cells is gradually established
74 during Treg cell development, and Treg-specific chromatin interactions were associated
75 with Treg signature gene expression. Furthermore, through comparison of WT Treg cells
76 with “wannabe” Treg cells (isolated from Foxp3-GFP knock-in/knockout mouse), and
77 Foxp3 domain-swap mutant (DSM) Treg cells (isolated from a newly-generated Foxp3
78 DSM mouse strain), our data showed that Foxp3 was critical for the establishment of
79 Treg-specific chromatin interactions, although not likely dependent on the Foxp3 domain-
80 swapped dimer to form Foxp3-associated chromatin loops. Our results revealed a
81 previously unappreciated aspect of Foxp3 function in the regulation of Treg cell
82 development and function.

83

84 **RESULTS**

85 **Global transformation of 3D genome architecture during Treg lineage specification**

86 To map the trajectory of the 3D genome organization during Treg lineage
87 development, we performed *in situ* Hi-C experiments with T cells in different
88 developmental stages, including CD4⁻CD8⁻ (DN), CD4⁺CD8⁺ (DP), CD4⁻CD8⁺ (CD8SP),
89 CD4⁺CD8⁻Foxp3⁻CD25⁻ (CD4SP), CD4⁺CD8⁻Foxp3⁻CD25⁺ (CD25⁺ Treg precursor),
90 CD4⁺CD8⁻Foxp3^{lo}CD25⁻ (Foxp3^{lo} Treg precursor), CD4⁺CD8⁻Foxp3⁺CD25⁺ (Treg) from
91 the thymus, and CD4⁺Foxp3⁻ (conventional T cells, Tcon) and CD4⁺Foxp3⁺ (mature Treg)
92 from the spleen (Figure 1A and Supplementary Fig. 1). Chromatin interaction maps were
93 constructed from Hi-C data at different resolutions down to 2kb resolution (Figure 1B). To
94 examine patterns of gains and losses of chromatin interactions, we performed K-means
95 clustering on normalized Hi-C contacts across each T cell population at 100kb resolution
96 (Figure 1C). This revealed evidence for both gains and losses of chromatin interactions
97 throughout the T cell developmental trajectory (Figure 1C,D). We next use T-distributed
98 Stochastic Neighbor Embedding (t-SNE) map to visualize and compare different T cell
99 subsets in two dimensions. t-SNE showed tight grouping between replicate experiments
100 from the same T cell subset, indicating high reproducibility of the chromatin contact maps.
101 Furthermore, the t-SNE map clearly showed a differentiation trajectory of Treg cell
102 development in the thymus, in parallel to the trajectory generated based on gene
103 expression profile of each T cell subset (Figure 1E). Therefore, the 3D genome structure
104 is being reorganized following the differential steps of thymic Treg cell development.

105

106 **Treg-specific chromatin contacts are associated with Treg gene expression and**
107 **selective transcription factor binding activities.**

108 To examine whether Treg cells have a unique 3D chromatin structure to support
109 their distinct gene expression profile and function, we performed a pairwise comparison
110 of the 3D chromatin structure of splenic Treg and Tcon cells. Using edgeR to detect
111 differential chromatin contacts at 25 kB resolution, we identified 1959 upregulated DNA
112 interactions in Treg cells and 1973 upregulated DNA interactions in Tcon cells (Figure
113 2A). As an example, we observed strong DNA interactions close to the *Socs2* gene locus
114 in Treg cells, but not in conventional T cells (Figure 1B). The Hi-C data showed that a
115 vast majority of DNA interactions were similar between Treg and Tcon, with only 0.29%
116 of tested chromatin interactions showing a significant change between Treg and Tcon
117 cells (3932/1377570). This small percentage agreed with previous studies showing that
118 less than 5% of the genes are differentially expressed in these two T cell
119 populations^{19,29,30}. Additionally, Treg and Tcon cells share 99% of their enhancers, less
120 than 1% of the enhancers are unique to either T cell population²⁶.

121 We next examined whether the differences in 3-D chromatin structures between
122 Treg and Tcon cells are associated with changes in gene expression. Analysis of gene
123 expression profiles of Treg and Tcon cells revealed that 928 genes (FDR > 1% and Fold
124 change > 2) were differentially expressed (Figure 2C). Based on Hi-C data, of the 3932
125 differential chromatin interactions between Treg and Tcon cells, 617 chromatin interaction
126 anchors overlapped with the transcription start site of at least one gene. Strikingly, ~35%
127 of these anchors contained differentially expressed genes (216 of 617), which accounted
128 for about one-quarter of all differentially expressed genes (216 of 928) (Figure 1D). This
129 result suggested that differences in gene expression are potentially associated with
130 unique DNA interacting activities in Treg cells.

131 To further explore the link between chromatin interactions and gene expression,
132 we determined the number of differential interacting partners for each individual
133 interaction anchor that is proximal to a differentially expressed gene. While most loci with
134 differential interactions had only one partner anchor, a minority of loci form multiple
135 differential long-range contacts (Figure 2E). We observed that the loci with higher
136 numbers of differential long-range interactions were more likely to be associated with
137 differentially expressed genes (Figure 2F and 2G). Of note, the loci with more than 4
138 differential DNA interactions were associated with several well-established Treg signature
139 genes, including *Ikzf2*, *Lrrc32* (encoding GARP), *Socs2*, and *Ptger4* (Figure 2G and 2H).
140 These results further illustrated the correlation between changes in DNA interactions and
141 differential gene expression in Treg cells.

142 To search for factors involved in establishing a Treg-specific 3D chromatin
143 structure, we compared the relative enrichment of several transcription factors and
144 chromatin structure regulators in Treg- and Tcon- specific loop anchors. Although CTCF
145 and cohesin are critical for the formation of DNA loops^{31,32}, their relative enrichments in
146 Tcon or Treg-specific loop anchors were moderate (Figure 2I). In contrast, multiple
147 transcription factors, including *Foxp3*, *Satb1*, *Runx1*, *Ets1*, and *Bcl11b*, which are
148 involved in Treg differentiation and function, showed a more pronounced enrichment in
149 Tcon or Treg-specific interactions. Strikingly, the enrichment of *Foxp3* bound peaks was
150 ranked first among all the transcription factors tested, suggesting that *Foxp3* might play
151 a crucial role in Treg-specific loop formation (Figure 2I).

152

153 **Foxp3 is critical for the establishment of Treg-specific 3D chromatin structure**

154 Foxp3 is a pivotal regulator of Treg differentiation and function. Given that Foxp3
155 bound peaks are highly enriched in the anchor regions of Treg-specific chromatin
156 interactions, we examined Foxp3's role in the formation and maintenance of Treg-specific
157 DNA loops. To this end, we used a GFP knock-in Foxp3 knockout mouse strain
158 (Foxp3^{GFP-KIKO})³⁰, in which GFP expression replaces Foxp3 and can be used as a
159 fluorescent marker to identify Treg “wannabe” cells (Figure 3A). Hi-C experiments were
160 performed with GFP⁺Foxp3⁻ Treg- “wannabe” cells from Foxp3^{GFP-KIKO} mice and control
161 GFP⁺Foxp3⁺ WT Treg cells from Foxp3^{GFP} mice. We focused on chromatin contacts that
162 were Treg specific in our comparison of Treg and Tcon chromatin interactions.
163 Comparison between the chromatin contacts in GFP⁺Foxp3⁺ WT Treg cells and
164 GFP⁺Foxp3⁻ Treg “wannabe” cells showed that a total of 124 out of 1569 Treg-specific
165 interactions were significantly reduced in the GFP⁺ Foxp3-KIKO cells (Figure 3B,
166 FDR=10%). While this represents a minority of the Treg-specific contacts (7.9% or
167 124/1569), the decrease in Treg-specific DNA contacts in Foxp3 KIKO cells was also
168 illustrated by the overall distributions of KIKO vs. WT contact frequency fold-changes
169 (Figure 3C). Specifically, 77.7% (1219/1569) of Treg-specific contacts showed a
170 decrease (fold change < 0) in chromatin interaction frequency in GFP⁺ Foxp3-KIKO cells
171 relative to control GFP⁺Foxp3⁺ WT Treg cells. The reduction of chromatin interactions in
172 GFP⁺Foxp3⁻ Treg- “wannabe” cells could be seen at the locus of the *Ikzf2* gene, one of
173 the Treg signature genes. In Tcon cells, there were no detectable chromatin interactions
174 around *Ikzf2*, while strong DNA interacting loops emerged in WT Treg cells. In the Treg-
175 “wannabe” cells, the chromatin interactions were significantly weakened at the *Ikzf2* locus
176 (Figure 3D). ChIP-seq and Cut&Run experiments showed the DNA looping anchors

177 around *Ikzf2* were enriched with Foxp3 bound peaks along with CTCF and cohesin
178 component Smc1a bound peaks (Figure 3E). The fact that some but not all Treg specific
179 chromatin interactions lost in GFP⁺Foxp3⁻ Treg- “wannabe” cells led us to investigate
180 whether contacts lost in GFP⁺Foxp3⁻ Treg- “wannabe” cells may be more dependent on
181 Foxp3. Indeed, chromatin contacts that were lost in the Treg- “wannabe” cells compared
182 to controls were more likely to contain Foxp3 binding peaks (Figure 3F). In addition to
183 Foxp3 binding sites, we also examined the enrichment of transcription factor (TF) motifs
184 in Treg DNase I Hypersensitive Sites (DHS), and identified motifs with differential TF motif
185 enrichment in chromatin contacts lost versus retained in GFP⁺Foxp3⁻ Treg- “wannabe”
186 cells versus control cells (Figure 3G). Specifically, we saw modest enrichments of CTCF,
187 ETS-family, and MEF2B/D TF motifs in DHS sites at chromatin contacts retained in
188 GFP⁺Foxp3⁻ Treg- “wannabe” cells. This suggests that these TFs, in conjunction with
189 Foxp3, may be critical for the establishment of the mature Treg 3D chromatin landscape.
190 Taken together, these data suggest that the establishment of Treg-specific chromatin
191 interactions is dependent on Foxp3 expression.

192

193 **Mutations in the Foxp3 domain-swapped dimerization interface lead to inadvertent**
194 **immune system activation in mice.**

195 Although our data clearly indicated that Foxp3 is indispensable for establishing
196 Treg-specific 3D chromatin structure, it is not clear whether Foxp3 is directly involved in
197 DNA looping like CTCF/cohesin, or whether it acts indirectly as a factor that facilitates the
198 binding of architectural proteins including CTCF and cohesin to form Treg-specific
199 chromatin interactions. It was reported that Foxp3 is able to form a domain-swap (DS)

200 dimer through its forkhead domain to bring two distal DNA elements together²⁸,
201 suggesting Foxp3 has the potential to facilitate DNA looping directly (Figure 4A). To test
202 this possibility, we generated a Foxp3 domain-swapped mutant (DSM) mouse strain by
203 using the CRISPR technology. Three amino acid mutations (W348Q, M370T and A372P)
204 were introduced to the Foxp3 coding region in the Foxp3-IRES-Thy1.1 reporter mouse
205 (Figure 4B). After verifying the mutations by DNA sequencing, we analyzed Foxp3 DSM
206 mice and WT littermate controls to determine whether disabling Foxp3's domain swapped
207 dimerization affects Treg cell development and function. The Foxp3 DSM mice appeared
208 to be normal up to 2 months of age when they started to develop a moderate
209 lymphoproliferative disease with loss of body weight and increased cellularity in the
210 spleen (Figure 4C, D). The frequency of Treg cells was higher while Foxp3 protein level
211 was significantly reduced in Foxp3 DSM mice compared to WT controls (Figure 4E).
212 CD4⁺ conventional T cells and CD8⁺ T cells were also more activated with the expansion
213 of the CD44⁺CD62L^{low} population. (Figure 4F). Consistently, IFN γ production increased
214 significantly in splenic CD4⁺ T cells from Foxp3 DSM mouse (Figure 4G). Furthermore,
215 serum concentrations of IgG1 and IgM were significantly higher in Foxp3 DSM mice
216 compared to WT controls (Figure 4H). Histopathology analysis of 6- to 9-month-old Foxp3
217 DSM mice revealed widespread immune cell infiltration in the lung, liver, small intestine,
218 and salivary gland tissues (Figure 4I). Taken together, these data suggested that the
219 inability of Foxp3 to dimerize in "trans" leads to a moderate defect in Treg cell's immune
220 suppressive function which results in excessive immune system activation.

221

222 **The formation of Treg-specific chromatin interactions is independent of Foxp3**
223 **domain-swap dimerization**

224 Next, we sought to assess whether the impairment of Foxp3 DSM Treg function
225 was because domain-swap mutation disrupted the formation of Treg 3D genome structure,
226 and subsequently affected Treg signature gene expression. To this end, we isolated Treg
227 cells from 6-week-old asymptomatic Foxp3 DSM and control mice and performed in-situ
228 Hi-C experiments to map their 3-D genome structure. Foxp3 DSM and WT Treg cells
229 showed similar chromatin interaction patterns as a whole and within Treg-specific
230 interactions (Figure 5A). In fact, none of the 1445 Treg specific chromatin interactions is
231 significantly different in the DSM Tregs compared to the WT Tregs (FDR<10%) (Figure
232 5B). Furthermore, we did not observe a global loss of chromatin contacts at Treg-specific
233 interactions in the DSM Treg cells as we do in the GFP⁺ Foxp3 KIKO cells (Figure 5C).
234 Finally, the lack of differences in 3D structure between DSM and WT Tregs was not
235 related to statistical power or data quality, as the sequencing depth and Hi-C library quality
236 was comparable between Tcon, Treg, KIKO, and DSM experiments (Supplementary
237 Table 1). Taken together, these results show that domain-swapped dimerization of Foxp3
238 is not required for establishing Treg-specific 3-D genome structure.

239 To further dissect the molecular mechanism underlying DSM Treg's impaired
240 function, we performed RNA-seq experiments with DSM and WT Treg cells. There were
241 26 up-regulated genes and 121 down-regulated genes in DSM Tregs compared to WT
242 Tregs (Figure 5D, FDR 5%, greater than 2-fold change). Interestingly, the differentially
243 expressed genes in the DSM Treg cells showed expression patterns resembling naïve T
244 cells, rather than WT Treg cells (Figure 5E), suggesting that the domain-swap mutation

245 disrupts Foxp3's transcriptional regulation function of Foxp3. The expression of several
246 Treg signature genes, *Lrrc32* (encodes the GARP protein), *Tigit*, and *Ctla4*, were
247 compromised in DSM Tregs, contributing to their impaired immune suppressive function.

248 To further explore the mechanism underlying dysregulated gene expression in
249 DSM Tregs despite the lack of changes in 3D genome structure, we examined whether
250 the DSM mutation contributed to differences in Foxp3 binding using CUT&RUN. We
251 identified 36,727 Foxp3 binding peaks in WT and DSM Tregs by CUT&RUN. Comparing
252 peak strength between WT and DSM-mutant Tregs, we identified 295 peaks that showed
253 differential Foxp3 binding (Figure 5F, FDR 5%). We then analyzed differential Foxp3
254 binding peaks based on their distance to differentially expressed genes in WT and DSM
255 Tregs. The differential DSM Foxp3 binding peaks were significantly closer to DEGs
256 compared to non-affect Foxp3 binding peak controls (Figure 5G). For example, although
257 chromatin interactions around *Lrrc32* were similar, the main Foxp3-bound peak was
258 weaker in DSM Tregs compared to WT controls (Figure 5H, 5I). It is likely that defective
259 Foxp3 binding resulted in the reduced expression level of *Lrrc32* in DSM Tregs (Figure
260 5J). Taken together, these results suggest that the domain-swapped mutation negatively
261 affects Foxp3 binding to the loci of a subset of genes, leading to compromised gene
262 expression and defective Treg function.

263

264 **Foxp3-associated chromatin interactions are functionally required for Treg cell** 265 **function**

266 To further understand how Foxp3 is involved in the establishment of Treg-specific
267 chromatin interaction, we performed proximity ligation-assisted ChIP-seq (PLAC-seq)³³

268 with an antibody against Foxp3 in Treg cells, which enabled us to analyze Foxp3-
269 associated chromatin interactions with higher sensitivity and efficiency. Using Foxp3
270 PLAC-seq data, we identified focal loops at 10 kB resolution. These focal loops were
271 highly overlapped with Foxp3 binding peaks in Treg cells (Figure 6A). In total, we
272 identified 2169 Foxp3-associated loop anchors, of which the majority contained a Foxp3
273 binding site or had a Foxp3 binding site within 10 kB (Figure 6B). Of note, 9.01% of the
274 total Foxp3 binding sites are associated with chromatin interactions identified by Foxp3
275 PLAC-seq (Figure 6C). We next classified Foxp3-associated DNA loops based on the
276 locations of the loop anchors relative to genes. More than two-thirds of the loops are
277 gene-gene (22.49% vs. expected 4.35%), gene-enhancer (27.12% vs expected 2.61%),
278 enhancer-enhancer (17.17% vs. expected 1.14%) interactions, implicating their
279 involvement in the regulation of gene expression (Figure 6D).

280 To examine how Foxp3-associated chromatin interactions influence gene
281 expression, we compared the expression of genes whose transcription starting site
282 overlaps with Foxp3 PLAC-seq interactions between CD4⁺ conventional T cells and
283 Tregs. A number of Treg signature genes, including *Ikzf2*, *Icos*, *Entpd1*, and *Il7r*, emerged
284 as associated with Foxp3 PLAC-seq interactions (Figure 6E). We next directly tested
285 whether Foxp3-associated chromatin loops facilitate gene expression at the *Ikzf2* locus.
286 Using a pair-guide RNA mediated CRISPR/Cas9 approach³⁴, we systemically deleted 9
287 Foxp3 binding sites (named P1 to P9) located close to the *Ikzf2* gene, and measured
288 Helios protein (encoded by the *Ikzf2* gene) expression in Treg cells compared to cells
289 transduced with non-targeting sgRNAs (Figure 6F and Supplementary Fig. 2). When the
290 Foxp3 binding site at the P1 or P6 regions were deleted, Helios expression decreased

291 significantly (Figure 6G). The P6 region is located in the *Ikzf2* promoter, therefore its
292 deletion served as a positive control. We next deleted the P1 or P6 region in mature
293 splenic Treg cells *in vitro*, which were then transferred into Rag1 knockout recipient mice
294 to track deletion's impact on Tregs *in vivo*. Indeed, Helios expression was reduced in
295 Tregs isolated from P1 deleted Treg cells (Figure 6H), suggesting that the P1 region is a
296 Foxp3 bound enhancer. Interestingly, Hi-C analysis showed that P1 deletion did not
297 significantly weaken Foxp3 PLAC-seq peak at the *Ikzf2* locus (Figure 6I). This data
298 suggests that Foxp3 may not be required for the maintenance of Treg-specific chromatin
299 interactions, despite that Foxp3 binding is essential for *Ikzf2* expression.

300 To further characterize Foxp3's role in the maintenance of Treg-specific chromatin
301 interactions in mature Treg cells, we used CRISPR/Cas9 to knockout Foxp3 in splenic
302 Treg cells *in vitro*, and profiled their 3D genome structure by *in situ* Hi-C (Supplementary
303 Fig. 3A, B). Unlike GFP⁺Foxp3⁻ KIKO cells, the deletion of Foxp3 by sgRNA in mature
304 Treg cells did not change their chromatin interaction patterns as a whole or within Treg-
305 specific interactions (Supplementary Fig. 3C). There was no global loss of chromatin
306 contacts at Treg-specific interactions in the sgFoxp3 Treg cells as in the GFP⁺ Foxp3⁻
307 KIKO cells (Supplementary Fig. 3D). Therefore, Foxp3 is essential for establishing Treg-
308 specific chromatin interactions but dispensable for the maintenance of these interactions
309 in mature Treg cells.

310 To further investigate Foxp3's role in Treg gene expression, we compared Treg-
311 specific genes, which are differentially expressed between Treg and Tcon cells, with
312 genes that are dysregulated in either the KIKO or DSM Treg cells. This divided the Treg-
313 specific genes into two sets, "Foxp3 dependent" (changing in KIKO or DSM or both) and

314 Foxp3 independent (not changing in KIKO or DSM) (Figure 7A). Gene Ontology (GO)
315 analysis of these two sets of genes revealed distinct GO terms. For the Foxp3-dependent
316 genes, the top terms were related to immune function, cytokines, and cell adhesion
317 (Figure 7B). For the Foxp3 independent genes, the top hits were related to metabolism
318 and cell cycle (Figure 7C). This was not caused by a specific p-value threshold, because
319 by comparing the GO terms obs/exp gene sets, there were a large number of GO terms
320 that were specific to the Foxp3 dependent or independent set (Figure 7D). Furthermore,
321 about 3/4 of all the GO terms that came up as significant in either the foxp3 dependent or
322 independent sets are specific to each set (Figure 7E). These analyses suggested that
323 Foxp3 regulates genes related to the immune function of Treg cells, while other factors
324 regulate cell cycle and cell metabolic processes during Treg lineage commitment.

325

326 **DISCUSSION**

327 In this study, we examined the role of Treg lineage-specific transcription factors
328 Foxp3 in 3D genome organization during the late stage of T cell development. We
329 compared the 3D chromatin structures of Treg cells and their precursors and revealed
330 that the 3D chromatin architecture of Treg cells was gradually established during Treg
331 lineage specification, and that changes in chromatin interactions align with the trajectory
332 of Treg development. By comparing Treg cells and their closely related conventional T
333 cells, we identified chromatin structures unique to Treg cells. Overall, the Treg's
334 chromatin structure was highly similar to that of conventional T cells, 0.29%
335 (3932/1377570) chromatin interactions were significantly different between Treg and
336 Tcon cells. This small number of differential chromatin interactions are in line with less

337 than 1% of differential enhancers, and less than 5% of differentially expressed genes
338 between Treg and conventional T cells. Strikingly, these Treg-specific chromatin
339 interactions were frequently associated with the loci of Treg signature genes.

340 Our study investigated Foxp3's contribution to the establishment and maintenance
341 of Treg's chromatin structure. Notably, Foxp3 was significantly enriched at the anchor
342 regions of Treg-specific chromatin loops, even ranking higher than CTCF/cohesin. By
343 taking advantage of Treg-“wannabe” cells from Foxp3^{GFP-KIKO} mice, our data revealed that
344 Foxp3 was essential for the establishment of Treg-specific chromatin structure, which
345 agreed with a recently published Foxp3 HiChIP study²⁷. It was proposed that the domain-
346 swapped dimer of Foxp3 facilitates its potential role as a DNA loop anchor to establish
347 Treg-specific chromatin interactions²⁸. We further examined whether Foxp3 can function
348 as a DNA loop anchor by comparing of WT and DSM Treg cells. Although the Foxp3 DSM
349 Treg cells were dysfunctional and the Foxp3 DSM mice developed lymphoproliferative
350 disease, the 3D chromatin architecture of the Treg cells was not affected by mutations
351 disrupting Foxp3 domain-swapped dimerization. Instead, the defective function of DSM
352 Tregs is likely caused by impaired Foxp3 binding to key Treg gene loci. Furthermore, a
353 recent study showed that the Foxp3 domain-swapped dimer is dysfunctional, while a
354 head-to-head dimer represents the physiological form of Foxp3³⁵. Altogether, these data
355 suggested that domain-swapped dimerization of Foxp3 is not required for the organization
356 of Treg's 3D chromatin structure.

357 The Foxp3 PLAC-seq and Foxp3 ChIP-seq/CUT&RUN data also revealed that
358 Foxp3-associated chromatin interactions were associated with the loci of Treg-signature
359 genes, including *Ikzf2*, *Icos*, *Entpd1*, and *Il7r*. Although the deletion of Foxp3 binding sites

360 in the *Ikzf2* locus decreased its expression, it did not disrupt the chromatin interactions at
361 the corresponding regions. Furthermore, the ablation of *Foxp3* in mature Treg cells did
362 not alter their 3D genome structure. This data indicates that although *Foxp3* plays an
363 essential role in the formation of Treg-specific chromatin interactions, it is not required for
364 their maintenance of the Treg's 3D chromatin structure. Furthermore, by comparing WT
365 Treg, "wannabe" Treg, and DSM Treg gene expression, we found that Treg-characteristic
366 genes can be separated into *Foxp3*-dependent and *Foxp3*-independent groups, with
367 *Foxp3*-dependent genes enriched in Treg immune suppressive functions, while *Foxp3*-
368 independent genes enriched in metabolic and cell cycle regulations.

369 In summary, our data suggest that *Foxp3* as a Treg lineage-specific transcription
370 factor facilitates chromatin structure reorganization to establish Treg's cell identity. Since
371 *Foxp3* by itself does not function as a chromatin loop anchor to stabilize chromatin
372 interactions, it likely cooperates with other proteins such as CTCF, cohesin, and YY1³⁶ to
373 set up Treg-specific 3D genome structure during Treg development. Once the 3D genome
374 structure is formed in mature Tregs, *Foxp3* is not required for its maintenance. Instead,
375 *Foxp3* acts as a transcription factor to activate or repress gene expression by leveraging
376 the promoter-enhancer proximity facilitated by the Treg-specific chromatin looping
377 structure. This study presented a model of how lineage-specific transcription factors
378 function during the late or terminal stage of cell differentiation.

379

380 **Acknowledgments**

381 We would like to thank T. Hua, N. Tessler, and C. Gordon for mouse colony management,
382 C. O'Connor for assistance in flow cytometry, Y. Dayn for assistance in generating the
383 Foxp3 DSM mutant mice. Z.L. was supported by a NOMIS Fellowship. D.S.L. was
384 supported by the 2022 Advanced Facility Fund of the University of Seoul. Y.Z. was
385 supported by the NOMIS Foundation, the Crohn's and Colitis Foundation, the Sol
386 Goldman Trust, and National Institutes of Health (R01-AI107027, R01-AI1511123, R21-
387 AI154919, and S10-OD023689). J.R.D. was supported by National Institutes of Health
388 (DP5-OD023071 and U01-CA260700). This work was also supported by National Cancer
389 Institute funded Salk Institute Cancer Center Core Facilities (P30-CA014195).

390

391 **Author Contributions**

392 Conceptualization: Z.L., D.L., Y.Z., and J.R.D. Methodology: Z.L. and D.L. Investigation:
393 Z.L., D.L., and Y.L. Resources: Y.Z. and J.R.D. Formal analysis: Z.L., D.L., and J.R.D.
394 Data Curation: Z.L. D.L., and J.R.D. Supervision: Y.Z. and J.R.D. Funding acquisition:
395 Y.Z. and J.R.D. Writing – original draft preparation: Z.L., D.L., Y.Z., and J.R.D. Writing –
396 review and editing: Z.L., D.L., Y.Z., and J.R.D.

397

398

399 **Figure Legends**

400 **Figure 1. Chromatin architecture reorganization during T cell lineage commitment.**

401 A) Schematic of experimental design to study changes in chromatin architecture during T
402 cell lineage commitment. B) Example Hi-C heat maps in mature splenic Treg cells at
403 progressively higher resolutions near the Bcl11b gene. C) Clustering of chromatin
404 interactions in thymic T cell subsets. Chromatin interactions were calculated at a
405 resolution of 100kb and clustered using K-means clustering (K=10). Replicate
406 experiments were also clustered using hierarchical clustering. D) Hi-C chromatin
407 interactions over specific loci that gain or lose chromatin contacts during T cell lineage
408 commitment. E) T-distributed stochastic neighbor embedding (tSNE) of chromatin
409 contacts (left panel) and gene expression (right panel) during T cell lineage commitment.

410

411 **Figure 2. Chromatin conformation changes between Treg cells and conventional**

412 **CD4+ T cells.** A) Chromatin interaction frequency of 25kb bins compared between
413 conventional CD4+ T cells (x-axis) and Treg cells (y-axis). Interactions called as
414 differential between Treg and Tcon cells are labelled red (FDR 1%). B) Hi-C browser shot
415 of a region showing Treg specific interactions. The Hi-C plot shows interactions over a
416 ~800kb locus containing a cluster of Treg upregulated genes (Plxnc1, Socs2, Ube2n,
417 Nudt4). Below the Hi-C data is a genome browser track of ChIP-seq for CTCF (green),
418 Smc1a (purple), H3K27ac (blue), and Foxp3 (orange, showing ChIP-seq and Cut&Run)
419 in Treg and Tcon cells. C) Plot of transcript abundance (x-axis) versus fold change (y-
420 axis) of gene expression between CD4+ Tcon cells and Treg cells. Points show in red are
421 called as differentially expressed genes (FDR 1%, minimum 2-fold change). D) Venn

422 diagram showing overlap between regions of the genome showing differential chromatin
423 contacts (purple) and the transcription start site of genes showing Treg specific
424 expression (green) (p-value by Fisher's exact test). E) Histogram of the number of
425 differential interacting partners for each differential interaction anchor. Most loci are
426 involved in differential interactions with one partner anchor, but a minority of loci form
427 multiple differential long-range contacts. F) Fraction of anchors of differential chromatin
428 interactions that overlap differentially expressed genes for loci involved in one or more
429 differential interactions. Loci involved with multiple differential long-range interactions are
430 more likely to contact differentially expressed genes. G) Heat map of genes overlapping
431 anchors involved in >4 differential chromatin interactions (log₂ fold-change). H) Example
432 of multi-way long-range differential chromatin interaction. Treg chromatin interactions are
433 shown in the upper right hand portion of the heat map, and Tcon chromatin interactions
434 are shown in the lower left hand portion of the heat map. I) Enrichment of ChIP-seq peaks
435 over differential chromatin interactions. ChIP-seq data is shown either from CD4⁺ Tcon
436 cells (pink box) or Treg cells (blue box). Enrichment is shown for Tcon specific interactions
437 (yellow bars) or Treg specific interactions (blue bars).

438

439 **Figure 3. Foxp3 is required for the complete establishment of Treg specific 3D**
440 **chromatin structure.** A) Schematic of the Foxp3-GFP knock-in and the Foxp3-GFP (WT)
441 and Foxp3 knock-in/knock-out (KIKO) mice. eGFP is knocked into the Foxp3 locus in both
442 the Foxp3-GFP and KIKO mice. In KIKO mouse, the eGFP is followed by 3x stop codons
443 to prevent Foxp3 protein translation. B) Chromatin interaction frequency between WT and
444 KIKO Treg cells at N=1569 Treg specific chromatin interactions. Treg specific chromatin

445 interactions were identified by comparison of splenic Treg and Tcon cells as shown in
446 Figure 2. Differential chromatin interactions (N=125/1569) are labeled as points in red
447 (FDR = 10%). C) Violin plot of the log₂ fold-change in interaction frequency between
448 Foxp3 WT and KIKO Treg cells at Treg specific chromatin interactions. The median log₂
449 fold change is -0.24 (black dot) consistent with a loss of chromatin interactions in KIKO
450 Tregs at Treg specific chromatin interactions. D) Hi-C interaction maps at the *Ikzf2*/Helios
451 gene in Tcon, Treg, Foxp3 WT Treg, and Foxp3 KIKO Tregs (left to right). E) Chromatin
452 interactions in Treg cells at the *Ikzf2*/Helios locus and the associated ChIP-seq or
453 CUT&RUN experiments over the locus. F) Enrichment of Foxp3 CUT&RUN peaks over
454 Treg specific chromatin interactions that are either retained in KIKO cells (gray) or lost in
455 KIKO cells (blue) showing that the regions that lose chromatin interactions in Foxp3 KIKO
456 cells are more likely to have Foxp3 binding sites. G) Observed vs. expected motif
457 frequency in DNase I Hypersensitive sites overlapping chromatin interactions lost in
458 Foxp3 KIKO cells (x-axis) vs. chromatin interactions retained in Foxp3 KIKO cells (y-axis).
459

460 **Figure 4. Foxp3 domain swap mutant mice develop an autoinflammatory**
461 **phenotype.** A) Schematic of Foxp3 domain swap dimer. Two Foxp3 proteins interact as
462 a dimer (white and pink chains) binding to two DNA strands in a “trans” configuration.
463 Structure from PDB accession 3QRF. B) Strategy for generation of Foxp3 domain swap
464 mutant mice by CRISPR/Cas9. Two sgRNAs were used to cut off the endogenous
465 genomic fragment, and a synthesized single-strand DNA with domain swap mutation was
466 used to guide CRISPR/Cas9 mediated homology-directed repair. C-I) 6- to 9-month-old
467 Foxp3 DSM (n=13) and WT (n=5) littermate control mice were analyzed for C) Body

468 weight, D) spleen cellularity, E) Frequency of Foxp3⁺ Treg cells in total CD4⁺ T cells and
469 Foxp3 protein level. F) frequency of CD44⁺CD62l^{lo} cells in CD4⁺ Tcon and CD8⁺ T cells,
470 G) frequency of IFN γ ⁺ and IL-17⁺ cells in CD4⁺ Tcon cells. H) ELISA quantification of the
471 concentrations of IgG1, IgM, IgG2c, and IgA in serum. I) Representative hematoxylin and
472 eosin staining of small intestine, liver, kidney, and lung sections from WT and Foxp3 DSM
473 mice.

474

475 **Figure 5. Foxp3 domain swap mutant and its impact on 3D genome structure and**
476 **gene expression.** A) Hi-C chromatin interactions in wild-type (WT) Treg cells (x-axis) and
477 Foxp3 domain swap mutant (DSM) Treg cells (y-axis). Treg specific interactions between
478 Treg and Tcon cells are labeled in red. B) Plot of chromatin interaction frequency (x-axis)
479 versus log₂ fold change in chromatin interaction frequency (y-axis) between DSM and
480 WT Treg cells. Points shown in red are called as significant differential interactions (FDR
481 10%). C) Violin plot of the log₂ of the fold change in interaction frequency between Foxp3
482 WT and Foxp3 KIKO Treg cells (red) or between Foxp3 WT and Foxp3 DSM Treg cells
483 (green) over Treg specific chromatin interactions. The black dots show the median fold-
484 change. D) Volcano plot of RNA-seq expression data between DSM and WT Treg cells.
485 The x-axis shows log₂ fold change in expression, while the y-axis shows $-1 \cdot \log_{10}(p$ -
486 value). Points labeled in red are genes that are significantly differentially expressed
487 between DSM and WT Tregs (FDR 1%, 2 fold minimum change). E) Heat map of
488 expression in CD4⁺ Tcon cells and different WT or DSM mutant Treg cells over genes
489 differentially expressed between CD4⁺ Tcon cells and Treg cells. F) Foxp3 CUT&RUN
490 peak enrichment in Foxp3 WT Treg (x-axis) and Foxp3 DSM Treg (y-axis) cells. Points in

491 red (N=295) show significantly differential Foxp3 peaks (FDR 5%). G) Cumulative density
492 plot of the distance between differential Foxp3 peaks and differentially expressed genes
493 (purple) compared to the distance between all Foxp3 peaks and differentially expressed
494 genes (gray) showing that Foxp3 peaks affected by the DSM mutation are closer to DSM
495 dysregulated genes (p-value is calculated by Wilcoxon test). H) Chromatin interactions
496 near the *Lrrc32* gene in Foxp3 WT Treg cells (upper right) versus Foxp3 DSM Treg cells
497 (lower left). The dashed line box shows a distal enhancer with a Foxp3 peak with reduced
498 binding in DSM Treg cells. I) Enhancer in the dashed box from panel H showing the
499 reduction in Foxp3 binding in DSM Treg cells by Foxp3 CUT&RUN. J) Expression of
500 *Lrrc32* in Tcon, Treg, Foxp3 WT Treg, and Foxp3 DSM Treg cells showing reduced *Lrrc32*
501 expression in DSM Treg cells.

502

503 **Figure 6. Foxp3-associated chromatin interactions link distal enhancers to Treg**
504 **signature genes.** A) Chromatin contact map of Foxp3 PLAC-seq data near the T reg
505 specific genes *Tnfrsf25* and *Ifng*. Shown below the map are genome browser tracks of
506 H3K27ac ChIP-seq (blue) and Foxp3 CUT&RUN (orange). B) Pie chart showing the
507 fraction of Foxp3 PLAC-seq anchors that contain a Foxp3 binding site (yellow), are within
508 10kb of a Foxp3 binding site (+/- 1 bin, tan), or do not overlap with Foxp3 binding site
509 (grey). C) Plot showing the fraction of Foxp3 binding sites associated with PLAC-seq
510 interactions. The observed overlap (9.01%) is shown as a dashed line, while the
511 distribution of random overlaps (1000 iterations) is shown in grey. D) Pie chart showing
512 the fraction of Foxp3 PLAC-seq peaks that link genes (Gene), enhancers (Enh), or
513 unannotated regions (Un). Enhancers are defined as distal H3K27ac peaks. Unannotated

514 regions are sites that do not overlap gene transcription start sites or distal H3K27ac peaks.
515 E) Gene expression in CD4+ Tcon cells (x-axis) and Treg cells (y-axis) of genes whose
516 TSS overlaps with Foxp3 PLAC-seq interactions. Points shown in red are genes called
517 as differentially expressed between Treg and Tcon cells (FDR1%, 2-fold minimum
518 change). F) Foxp3 PLAC-seq data near the *Ikzf2*/Helios locus. Shown below the
519 interaction map are ChIP-seq and CUT&RUN tracks at the locus as well as the locations
520 of Foxp3 binding sites targeted for CRISPR deletion across the locus (P1-P9). G) The
521 effect of CRISPR deletion of Foxp3 binding sites P1 or P6 on Helios expression in Treg
522 cells in vitro. H) In vivo validation of the effect of P1 or P6 deletion on Helios expression.
523 Treg cells transduced with gRNAs targeting P1 or P6 were co-transferred with Tregs with
524 control gRNAs into the same Rag1^{-/-} mice, and Helios expression was then analyzed 2
525 weeks post transfer. I) Hi-C interaction map at the *Ikzf2*/Helios gene in Treg cells
526 transduced with control gRNAs (upper right) or gRNAs targeting P1 (lower left).

527

528 **Figure 7. Foxp3 dependence defines differential programs of Treg lineage**
529 **commitment.** A) Gene expression of genes differentially expressed between Tcon and
530 Treg cells across Foxp3 WT and mutant cells. Genes are separated into those that show
531 significant differences in the Foxp3 KIKO, DSM, or both mutants (“Foxp3 dependent”) and
532 those that show differential regulation in Tcon vs. Treg cells but do not show differences
533 in the Foxp3 mutant cells (“Foxp3 independent”). B) Gene ontology analysis of the “Foxp3
534 dependent” genes shows terms related to immune differentiation and function. C) Gene
535 ontology analysis of “Foxp3 independent” genes shows terms related to metabolic
536 regulation and the cell cycle. D) Comparison of the observed/expected Gene ontology

537 term frequency for Foxp3 dependent (x-axis) versus independent (y-axis) genes shows
538 an inverse correlation of enrichment of ontology terms. E) Pie chart of gene ontology
539 terms that are significant for either “Foxp3 dependent” or “Foxp3 independent” genes that
540 are significant in both sets (purple) or Foxp3 independent alone (red) or Foxp3 dependent
541 alone (blue).
542

543 **Supplementary Figure Legends**

544 **Supplementary Figure 1. Flow cytometry isolation of T cell populations in the**
545 **thymus and spleen.** A) Flow cytometric gating strategy to isolate T cells in the thymus,
546 including CD4⁻CD8⁻ (DN), CD4⁺CD8⁺ (DP), CD4⁻CD8⁺ (CD8SP), CD4⁺CD8⁻Foxp3⁻
547 CD25⁻ (CD4SP), CD4⁺CD8⁻Foxp3⁻CD25⁺ (CD25⁺ Treg precursor), CD4⁺CD8⁻
548 Foxp3^{lo}CD25⁻ (Foxp3^{lo} Treg precursor), CD4⁺CD8⁻Foxp3⁺CD25⁺ (Treg). B) Flow
549 cytometric gating strategy to isolate CD4⁺Foxp3⁻ (conventional T cells, Tcon) and
550 CD4⁺Foxp3⁺ (mature Treg) from the spleen.

551

552 **Supplementary Figure 2. CRISPR deletion of Foxp3 sites near the Ikzf2 gene.** A) Hi-
553 C chromatin interactions near the Ikzf2 gene. The heatmap shows Hi-C data near Ikzf2,
554 while the ChIP-seq tracks below show signals for CTCF and Foxp3 binding. Also labeled
555 are the locations of the 9 deleted Foxp3 sites (P1-P9). B) Flow cytometric analysis of the
556 expression of Helios after CRISPR knockout of indicated Foxp3-bound sites (Ikzf2 P1-P9)
557 in Treg cells.

558

559 **Supplementary Figure 3. CRISPR/Cas9 deletion of Foxp3 in mature Treg cells.** A)
560 Schematic of experimental strategy for deletion of Foxp3 in mature Treg cells. B) FACS
561 plots showing sgFoxp3 targeting efficiency in knockdown of Foxp3 expression in Treg
562 cells. C) Comparison of chromatin interactions between sgControl and sgFoxp3 targeted
563 Treg cells. The plot shows the strength of chromatin contacts (X-axis) and the fold change
564 in chromatin interaction frequency (y-axis) between sgControl and sgFoxp3 targeted cells.
565 Only one interacting locus shows a significant difference in interaction frequency (colored

566 in red). D) Violin plots of fold change in chromatin interaction frequency between mutant
567 and wild type comparing the effects in the Foxp3 KIKO Treg cells (left, orange) and in
568 Foxp3 sgRNA targeted cells (right, blue).

569

570 References

- 571 1 Lieberman-Aiden, E. *et al.* Comprehensive mapping of long-range interactions reveals
572 folding principles of the human genome. *Science* **326**, 289-293,
573 doi:10.1126/science.1181369 (2009).
- 574 2 Rao, S. S. *et al.* A 3D map of the human genome at kilobase resolution reveals principles
575 of chromatin looping. *Cell* **159**, 1665-1680, doi:10.1016/j.cell.2014.11.021 (2014).
- 576 3 Dixon, J. R. *et al.* Topological domains in mammalian genomes identified by analysis of
577 chromatin interactions. *Nature* **485**, 376-380, doi:10.1038/nature11082 (2012).
- 578 4 Bonev, B. & Cavalli, G. Organization and function of the 3D genome. *Nat Rev Genet* **17**,
579 661-678, doi:10.1038/nrg.2016.112 (2016).
- 580 5 Schmitt, A. D., Hu, M. & Ren, B. Genome-wide mapping and analysis of chromosome
581 architecture. *Nat Rev Mol Cell Biol* **17**, 743-755, doi:10.1038/nrm.2016.104 (2016).
- 582 6 Dixon, J. R., Gorkin, D. U. & Ren, B. Chromatin Domains: The Unit of Chromosome
583 Organization. *Mol Cell* **62**, 668-680, doi:10.1016/j.molcel.2016.05.018 (2016).
- 584 7 Zheng, H. & Xie, W. The role of 3D genome organization in development and cell
585 differentiation. *Nat Rev Mol Cell Biol* **20**, 535-550, doi:10.1038/s41580-019-0132-4
586 (2019).
- 587 8 Stadhouders, R., Filion, G. J. & Graf, T. Transcription factors and 3D genome
588 conformation in cell-fate decisions. *Nature* **569**, 345-354, doi:10.1038/s41586-019-1182-
589 7 (2019).
- 590 9 Merckenschlager, M. & Nora, E. P. CTCF and Cohesin in Genome Folding and
591 Transcriptional Gene Regulation. *Annu Rev Genomics Hum Genet* **17**, 17-43,
592 doi:10.1146/annurev-genom-083115-022339 (2016).
- 593 10 Johanson, T. M. *et al.* Transcription-factor-mediated supervision of global genome
594 architecture maintains B cell identity. *Nat Immunol* **19**, 1257-1264, doi:10.1038/s41590-
595 018-0234-8 (2018).
- 596 11 Kim, S. & Shendure, J. Mechanisms of Interplay between Transcription Factors and the
597 3D Genome. *Mol Cell* **76**, 306-319, doi:10.1016/j.molcel.2019.08.010 (2019).
- 598 12 Hu, G. *et al.* Transformation of Accessible Chromatin and 3D Nucleome Underlies
599 Lineage Commitment of Early T Cells. *Immunity* **48**, 227-242 e228,
600 doi:10.1016/j.immuni.2018.01.013 (2018).
- 601 13 Wang, W. *et al.* TCF-1 promotes chromatin interactions across topologically associating
602 domains in T cell progenitors. *Nat Immunol* **23**, 1052-1062, doi:10.1038/s41590-022-
603 01232-z (2022).
- 604 14 Shan, Q. *et al.* Tcf1-CTCF cooperativity shapes genomic architecture to promote CD8(+)
605 T cell homeostasis. *Nat Immunol* **23**, 1222-1235, doi:10.1038/s41590-022-01263-6
606 (2022).
- 607 15 Sakaguchi, S. *et al.* Regulatory T Cells and Human Disease. *Annu Rev Immunol* **38**, 541-
608 566, doi:10.1146/annurev-immunol-042718-041717 (2020).
- 609 16 Josefowicz, S. Z., Lu, L. F. & Rudensky, A. Y. Regulatory T cells: mechanisms of
610 differentiation and function. *Annu Rev Immunol* **30**, 531-564,
611 doi:10.1146/annurev.immunol.25.022106.141623 (2012).

- 612 17 Hori, S., Nomura, T. & Sakaguchi, S. Control of regulatory T cell development by the
613 transcription factor Foxp3. *Science* **299**, 1057-1061, doi:10.1126/science.1079490
614 (2003).
- 615 18 Fontenot, J. D., Gavin, M. A. & Rudensky, A. Y. Foxp3 programs the development and
616 function of CD4+CD25+ regulatory T cells. *Nat Immunol* **4**, 330-336, doi:10.1038/ni904
617 (2003).
- 618 19 Fontenot, J. D. *et al.* Regulatory T cell lineage specification by the forkhead transcription
619 factor foxp3. *Immunity* **22**, 329-341, doi:10.1016/j.immuni.2005.01.016 (2005).
- 620 20 Williams, L. M. & Rudensky, A. Y. Maintenance of the Foxp3-dependent developmental
621 program in mature regulatory T cells requires continued expression of Foxp3. *Nat*
622 *Immunol* **8**, 277-284, doi:10.1038/ni1437 (2007).
- 623 21 Kwon, H. K., Chen, H. M., Mathis, D. & Benoist, C. Different molecular complexes that
624 mediate transcriptional induction and repression by FoxP3. *Nat Immunol*,
625 doi:10.1038/ni.3835 (2017).
- 626 22 Angelin, A. *et al.* Foxp3 Reprograms T Cell Metabolism to Function in Low-Glucose, High-
627 Lactate Environments. *Cell Metab*, doi:10.1016/j.cmet.2016.12.018 (2017).
- 628 23 Zheng, Y. & Rudensky, A. Y. Foxp3 in control of the regulatory T cell lineage. *Nat*
629 *Immunol* **8**, 457-462, doi:10.1038/ni1455 (2007).
- 630 24 Van Gool, F. *et al.* A Mutation in the Transcription Factor Foxp3 Drives T Helper 2
631 Effector Function in Regulatory T Cells. *Immunity* **50**, 362-377 e366,
632 doi:10.1016/j.immuni.2018.12.016 (2019).
- 633 25 Rudra, D. *et al.* Transcription factor Foxp3 and its protein partners form a complex
634 regulatory network. *Nat Immunol* **13**, 1010-1019, doi:10.1038/ni.2402 (2012).
- 635 26 Samstein, R. M. *et al.* Foxp3 exploits a pre-existent enhancer landscape for regulatory T
636 cell lineage specification. *Cell* **151**, 153-166, doi:10.1016/j.cell.2012.06.053 (2012).
- 637 27 Ramirez, R. N., Chowdhary, K., Leon, J., Mathis, D. & Benoist, C. FoxP3 associates with
638 enhancer-promoter loops to regulate Treg-specific gene expression. *Sci Immunol* **7**,
639 eabj9836, doi:10.1126/sciimmunol.abj9836 (2022).
- 640 28 Bandukwala, H. S. *et al.* Structure of a domain-swapped FOXP3 dimer on DNA and its
641 function in regulatory T cells. *Immunity* **34**, 479-491, doi:10.1016/j.immuni.2011.02.017
642 (2011).
- 643 29 Hill, J. A. *et al.* Foxp3 transcription-factor-dependent and -independent regulation of the
644 regulatory T cell transcriptional signature. *Immunity* **27**, 786-800,
645 doi:10.1016/j.immuni.2007.09.010 (2007).
- 646 30 Gavin, M. A. *et al.* Foxp3-dependent programme of regulatory T-cell differentiation.
647 *Nature* **445**, 771-775, doi:10.1038/nature05543 (2007).
- 648 31 Rao, S. S. P. *et al.* Cohesin Loss Eliminates All Loop Domains. *Cell* **171**, 305-320 e324,
649 doi:10.1016/j.cell.2017.09.026 (2017).
- 650 32 Nora, E. P. *et al.* Targeted Degradation of CTCF Decouples Local Insulation of
651 Chromosome Domains from Genomic Compartmentalization. *Cell* **169**, 930-944 e922,
652 doi:10.1016/j.cell.2017.05.004 (2017).
- 653 33 Fang, R. *et al.* Mapping of long-range chromatin interactions by proximity ligation-
654 assisted ChIP-seq. *Cell Res* **26**, 1345-1348, doi:10.1038/cr.2016.137 (2016).

- 655 34 Gilbert, L. A. *et al.* CRISPR-mediated modular RNA-guided regulation of transcription in
656 eukaryotes. *Cell* **154**, 442-451, doi:10.1016/j.cell.2013.06.044 (2013).
- 657 35 Leng, F. *et al.* The transcription factor FoxP3 can fold into two dimerization states with
658 divergent implications for regulatory T cell function and immune homeostasis.
659 *Immunity*, doi:10.1016/j.immuni.2022.07.002 (2022).
- 660 36 Weintraub, A. S. *et al.* YY1 Is a Structural Regulator of Enhancer-Promoter Loops. *Cell*
661 **171**, 1573-1588 e1528, doi:10.1016/j.cell.2017.11.008 (2017).
662
663

664 **Methods**

665 **Mice**

666 All mice were housed in a specific pathogen-free facility under a 12 h light/dark cycle, with
667 an ambient temperature of 20–26 °C and humidity of 30–70% at the Salk Institute. Animal
668 experiments were performed under the regulation of the Institutional Animal Care and
669 Use Committee according to the institutional guidelines. All mice used in the present study
670 are in the C57BL/6 genetic background. Rag1^{-/-} mice purchased from the Jackson
671 Laboratory were used for adoptive Treg cell transfer. Foxp3^{Thy1.1} reporter mice³⁷,
672 Foxp3^{GFP} reporter mice¹⁹, and Foxp3^{GFPKO} mice³⁸ were used to isolate T cell populations
673 from the thymus and Tcon and Treg cells from spleen for in-situ Hi-C, PLAC-seq,
674 CUT&RUN, and RNA-seq experiments. Rosa-Cas9/Foxp3^{Thy1.1} mice³⁹ were used to
675 isolate Treg cells for CRISPR validation of the effect of Foxp3-binding sites on Helios
676 expression.

677

678 **Generation of Foxp3 domain-swap mutant knock-in mice**

679 The Foxp3 domain-swap mutant mice were generated by CRISPR/Cas9-based genome
680 editing⁴⁰. Briefly, two sgRNAs containing the target sequences
681 gRNA1(TGAAAGGGGGTTCGCATATTG) and gRNA2 (AAACCACCCCGCCACCTGGA)
682 and Cas9 protein were used to introduce double-strand DNA breaks; a 1340 base pair
683 (bp) single-strand DNA (ssDNA) containing the sequence encoding the three amino acids
684 mutations (W348Q, M370T, A372P) was used to introduce Foxp3 domain-swap
685 mutations via homology-directed DNA repair mechanism. The gRNAs-Cas9 RNP
686 together with ssDNA were injected into fertilized eggs derived from the Foxp3^{Thy1.1}
687 reporter mice, and then transplanted into pseudo-pregnant recipient mice. The
688 genomic region surrounding the target sites was amplified from genomic DNA of resultant
689 founder progeny by PCR using the following primers: 5'-TCTGAGGAGCCCCAAGATGT-
690 3', 5'-CCACTCGCACAAAGCACTTG-3'. After verifying the Foxp3 domain-swap
691 mutations by sequencing, Foxp3 DSM mice were bred with Foxp3^{Thy1.1} mice and analyzed
692 to determine the outcomes of the Foxp3 domain-swap mutation. Details of the ssDNA
693 sequence are listed in Supplementary Table 1.

694

695 **T cell isolation and analysis**

696 DN, DP, CD8SP, CD4SP, CD25⁺ Treg precursor, Foxp3^{lo} Treg precursor, thymic Treg
697 cells were isolated by FACS sorting from a thymocyte suspension. Tcon and Treg cells
698 were isolated from the spleen by pre-enrichment with EasySep Mouse CD4⁺ T cell
699 Isolation Kit (STEMCELL Technologies, Cat# 19852), and FACS sorting. The individual
700 cell population was sorted by FACS using the following markers. DN: CD45⁺CD4⁻CD8⁻;
701 DP:CD45⁺CD4⁺CD8⁺; CD8SP: CD45⁺CD4⁻CD8⁺; CD4SP: CD45⁺CD4⁺CD8⁻CD25⁻
702 Foxp3-reporter⁻; CD25⁺ Treg precursor: CD45.2⁺CD4⁺CD8⁻CD25⁺Foxp3-reporter⁻;
703 Foxp3^{lo} Treg precursor: CD45⁺CD4⁺CD8⁻CD25⁻Foxp3-reporter^{low}; mature thymic Treg:
704 CD45⁺CD4⁺CD8⁻CD25⁺Foxp3-reporter⁺; Splenic Tcon cells: CD45⁺TCRb⁺CD4⁺CD8⁻
705 Foxp3-reporter⁻; splenic Treg cells: CD45⁺ TCRb⁺CD4⁺CD8⁻Foxp3-reporter (Thy1.1 or
706 GFP)⁺.

707

708 To analyze immune cell compositions in Foxp3 DSM mice, a single cell suspension was
709 prepared from the spleen or lymph nodes, treated with red cell lysis buffer, and filtered
710 through 70 μ m cell strainer. For transcription factor staining, cells were first stained for
711 surface markers, followed by fixation and permeabilization with reagents from the
712 Foxp3/Transcription Factor Staining Buffer Set (eBioscience, 00-5521-00) and incubated
713 with antibodies according to the manufacturer's protocol. For cytokine analysis, cells were
714 stimulated with phorbol 12-myristate 13-acetate (PMA) (50 ng ml⁻¹; Sigma), ionomycin
715 (500 ng ml⁻¹; Sigma) and GolgiStop (BD) for 5 hours. Cells were incubated with cell
716 surface antibodies on ice for 30 min, and then subjected to intracellular staining using
717 Foxp3/Transcription Factor Staining Buffer Set as described above. Samples were run
718 on a BD FACSAria II Flow Cytometer (Becton Dickinson) and data were analyzed by
719 FlowJo software (Tree Star).

720

721 ***In situ* Hi-C**

722 *In situ* Hi-C experiments were performed as previously described² using restriction
723 enzyme MboI (NEB) with minor modifications. Briefly, 0.5 \times 10⁶ cells per each
724 developmental stage from DN to mature thymic Treg cells, and 1 \times 10⁶ splenic Tcon and
725 Treg cells were FACS-sorted and collected for individual biological replicates. Cells were

726 resuspended in RPMI1640 medium at a concentration of 1×10^6 cells per mL, cross-linked
727 with 1% formaldehyde for 10 minutes at room temperature with rotating, and
728 subsequently lysed and digested with 100 Units of Mbol/1 million cells at 37 °C for 2 hours.
729 The following steps including making of DNA ends, proximity ligation and crosslink
730 reversal, DNA shearing and size selection, biotin pull-down and preparation for Illumine
731 Sequencing, final amplification and purification were carried out as previously described.
732

733 **CUT&RUN**

734 CUT&RUN experiments were performed as previously described⁴¹ with minor
735 modifications. To avoid the potential activation of T cells by Concanavalin-A (ConA)
736 beads in the standard protocol, we instead used a spin-down method to collect cells as
737 previously reported⁴². Briefly, 0.5×10^6 cells per biological replicate were collected in V-
738 bottom 96-well plate. Cells were first washed twice in Antibody Buffer (2mM EDTA, 1X
739 EDTA-free protease inhibitors, 0.5mM spermidine, 1x permeabilization buffer from
740 eBioscience™ Foxp3/Transcription Factor Staining Buffer Set) by centrifugation at
741 1900rpm for 6 min at 4°C, and then incubated with normal IgG, H3K27ac antibody, or
742 Foxp3 antibody on ice for 1 hour. After two washes with buffer 1 (1X EDTA-free protease
743 inhibitors, 0.5mM spermidine, 1x permeabilization buffer), cell pellets were incubated with
744 pA/G-MNase (20X) enzyme (EpiCypher) in 50µl buffer 1 at 4°C for 1 hour. Cells were
745 washed twice in saponin buffer (0.05% (w/v) saponin, 1X EDTA-free protease inhibitors,
746 0.5mM spermidine in PBS) and resuspended in 100µl calcium buffer (2mM CaCl₂ in buffer
747 2) on ice for 30 min. 100µl 2x stop buffer (20mM EDTA, 4mM EGTA in saponin buffer)
748 was then added and incubated at 37°C for 10-20 min to release cleaved chromatin
749 fragments. The supernatant containing chromatin fragments was collected by
750 centrifugation and DNA was extracted using a QIAGEN MinElute kit according to
751 manufacturer's protocol.

752 The CUT&RUN libraries were prepared using the NEBNext® Ultra™ II DNA Library Prep
753 Kit for Illumina® (E7645) according to manufacturer's instructions.

754

755 **PLAC-seq**

756 PLAC experiments were performed as previously described³³. Briefly, 20×10^6 cells per
757 biological replicate were crosslinked in 1% formaldehyde for 10 minutes at room
758 temperature. After digestion with the restriction enzyme MboI, labeling DNA ends with
759 biotin-14-dATP, and proximity ligation of DNA ends, the resultant chromatin was
760 sonicated to 200-600 bp using a Covaris E229 sonicator for 10 min. Sonicated chromatin
761 was pre-cleared with Protein A+G magnetic beads followed by overnight chromatin
762 immunoprecipitations with 5 μ g Foxp3 antibody. Libraries were prepared using NuGen
763 Ovation Ultralow Library System V2 kit according to the manufacturer's instructions and
764 sequenced by an Illumina HiSeq2500 sequencer.

765

766 **RNA-seq**

767 1×10^4 cells were FACS-sorted into TRIzol RNA isolation reagent (Invitrogen) and RNA
768 was isolated according to the protocol. RNA concentration and integrity was determined
769 by Bioanalyzer using RNA 6000 Pico Kit (Agilent). RNA-seq libraries were constructed
770 using Illumina TruSeq Stranded mRNA kit (Illumina) following manufacturer's instructions.

771

772 **Serum Immunoglobulin ELISA**

773 Serum IgG1, IgG2c, IgM, and IgA concentrations were measured by ELISA using the
774 SBA Clono-typing System (Southern Biotech).

775

776 **Histology**

777 For histology analysis, lung, liver, small intestine, and salivary gland tissues were fixed in
778 10% neutral buffer formalin, paraffin-embedded, sectioned, and stained with hematoxylin
779 and eosin by Pacific Pathology (San Diego, CA).

780

781 **In vitro culture of Treg cells**

782 Treg cells were isolated from spleen of the Foxp3^{Thy1.1} reporter mice by staining with PE-
783 labeled Thy1.1 antibody followed by enrichment with Anti-PE magnetic beads (Miltenyi,
784 Cat# 130-048-801). Purity of the Treg cells was confirmed to be over 95% by FACS. Treg
785 cells were activated by plate-bound anti-CD3 and anti-CD28 antibodies in complete
786 RPMI1640 medium containing 10% FBS, 100 U/ml Penicillin/Streptomycin, 1 X GlutaMax,

787 1 mM HEPES, 1 mM sodium pyruvate, 1X NEAA, 55 mM 2-mercaptoethanol, 10 mg/ml
788 gentamycin, and IL-2 at 500 U/ml.

789

790 **CRISPR knockout of Foxp3 binding sites in *Ikzf2* locus**

791 Cloning of sgRNAs into the pSIRG-NGFR vector, and retrovirus production in HEK293T
792 cells were performed as previously described⁴³. Details of sgRNA sequence are listed in
793 Supplementary Table 2.

794 To test the effects of Foxp3 binding sites on Helios expression *in vitro*, Treg cells isolated
795 from Rosa-Cas9/Foxp3^{Thy1.1} mice were transduced with retrovirus carrying the sgRNAs
796 targeting P1 region, P6 region, or control non-targeting sgRNAs. Cells were stained and
797 analyzed for Helios expression by FACS 5 days after transduction.

798

799 ***In vivo* adoptive Treg cell transfer**

800 To test the effect of Foxp3 binding sites in the *Ikzf2* locus on Helios expression *in vivo*,
801 Treg cells from Rosa-Cas9 mice were first transduced with control sgRNAs, sgRNAs
802 targeting P1 or P6 region on day 1, and then sorted by FACS on day 3 to enrich Treg
803 cells transduced with sgRNAs (CD4⁺Foxp3^{Thy1.1}+NGFR⁺). CD45.2⁺ Treg cells transduced
804 with control sgRNAs were mixed with CD45.1⁺CD45.2⁺ Treg cells transduced with
805 sgRNAs targeting P1 or P6 region respectively at a ratio of 50:50 into RAG KO mice. 2
806 weeks after transfer, T cells in the spleen were harvested for analysis of the expression
807 of Helios

808

809 **In-situ Hi-C and PLAC-seq data analysis**

810 Hi-C and PLAC-seq data were aligned to the mm9 reference genome using BWA-
811 MEM⁴⁴. Reads were filtered (MAPQ >= 30) and paired using a previously described
812 pipeline⁴⁵. PCR duplicate reads were removed using Picard. Contact matrices were
813 generated and normalized using the iterative correction method⁴⁶. Enriched contacts in
814 the PLAC-seq data were identified using HICCUPS⁴⁷.

815 To detect differential chromatin interactions between experiments, we calculated
816 contact frequencies in 25kb bins for all interactions genome wide separated by less than
817 1Mb. Differential interacting regions were called using edgeR⁴⁸ with Benjamini-Hochberg
818 correction for multiple testing.

819 Transcription factor motif enrichment in Foxp3-dependent chromatin interaction
820 sites was performed by first identifying differential chromatin interactions between wild-
821 type (Foxp3GFP+) and Foxp3 knockout (KIKO GFP+) Tregs at a resolution of 25kb.
822 Differential interacting regions were overlapped with DNase I Hypersensitive sites in
823 mouse Tregs from ENCODE (accession ENCF566TDU). Motif enrichment over these
824 DHS sites found in differential interaction regions was performed using Homer⁴⁹ using the
825 collection of known vertebrate motifs from the JASPAR database.

826 RNA-seq data analysis

827 RNA-seq data were aligned by using STAR⁴⁴ to the mm9 reference genome. PCR
828 duplicates were removed, and read counts were quantified over GENCODE genes (vM1)
829 using HTSeq and subject to RPKM normalization. Differentially expressed genes were
830 identified using edgeR⁴⁸. Gene Ontology analysis was performed using TopGO⁵⁰.

831

832 CUT&RUN data analysis

833 CUT&RUN data was aligned to the mm9 reference genome using BWA-MEM⁴⁴.
834 Peaks were called using MACS2⁵¹. Peaks calls from the Foxp3 experiments together to
835 create a union set of peaks. Using this merged peak set, we then identified differential
836 Foxp3 sites using edgeR⁴⁸.

837

838 Data availability

839 The sequencing data from the RNA-seq, ChIP-seq, CUT&RUN, Hi-C, and PLAC-seq
840 experiments have been deposited in Gene Expression Omnibus (GEO) with the following
841 accession ID: GSE217147. [<https://www.ncbi.nlm.nih.gov/geo/query/acc.cgi>]. Please use
842 the reviewer token “otkxesceztgvvkz”.

843

844 References for Methods

845

- 846 37 Liston, A. *et al.* Differentiation of regulatory Foxp3+ T cells in the thymic cortex. *Proc*
847 *Natl Acad Sci U S A* **105**, 11903-11908, doi:10.1073/pnas.0801506105 (2008).
848 38 Gavin, M. A. *et al.* Foxp3-dependent programme of regulatory T-cell differentiation.
849 *Nature* **445**, 771-775, doi:10.1038/nature05543 (2007).
850 39 Loo, C. S. *et al.* A Genome-wide CRISPR Screen Reveals a Role for the Non-canonical
851 Nucleosome-Remodeling BAF Complex in Foxp3 Expression and Regulatory T Cell
852 Function. *Immunity* **53**, 143-157 e148, doi:10.1016/j.immuni.2020.06.011 (2020).

853 40 Yang, H., Wang, H. & Jaenisch, R. Generating genetically modified mice using
854 CRISPR/Cas-mediated genome engineering. *Nat Protoc* **9**, 1956-1968,
855 doi:10.1038/nprot.2014.134 (2014).

856 41 Skene, P. J. & Henikoff, S. An efficient targeted nuclease strategy for high-resolution
857 mapping of DNA binding sites. *Elife* **6**, doi:10.7554/eLife.21856 (2017).

858 42 van der Veecken, J. *et al.* The Transcription Factor Foxp3 Shapes Regulatory T Cell Identity
859 by Tuning the Activity of trans-Acting Intermediaries. *Immunity* **53**, 971-984 e975,
860 doi:10.1016/j.immuni.2020.10.010 (2020).

861 43 Liu, Z. *et al.* Glucocorticoid signaling and regulatory T cells cooperate to maintain the
862 hair-follicle stem-cell niche. *Nat Immunol*, doi:10.1038/s41590-022-01244-9 (2022).

863 44 Li, H. Aligning sequence reads, clone sequences and assembly contigs with BWA-MEM.
864 *arXiv e-prints*, arXiv:1303.3997 (2013).

865 45 Dixon, J. R. *et al.* Integrative detection and analysis of structural variation in cancer
866 genomes. *Nat Genet* **50**, 1388-1398, doi:10.1038/s41588-018-0195-8 (2018).

867 46 Imakaev, M. *et al.* Iterative correction of Hi-C data reveals hallmarks of chromosome
868 organization. *Nat Methods* **9**, 999-1003, doi:10.1038/nmeth.2148 (2012).

869 47 Durand, N. C. *et al.* Juicer Provides a One-Click System for Analyzing Loop-Resolution Hi-
870 C Experiments. *Cell Syst* **3**, 95-98, doi:10.1016/j.cels.2016.07.002 (2016).

871 48 Robinson, M. D., McCarthy, D. J. & Smyth, G. K. edgeR: a Bioconductor package for
872 differential expression analysis of digital gene expression data. *Bioinformatics* **26**, 139-
873 140, doi:10.1093/bioinformatics/btp616 (2010).

874 49 Heinz, S. *et al.* Simple combinations of lineage-determining transcription factors prime
875 cis-regulatory elements required for macrophage and B cell identities. *Mol Cell* **38**, 576-
876 589, doi:10.1016/j.molcel.2010.05.004 (2010).

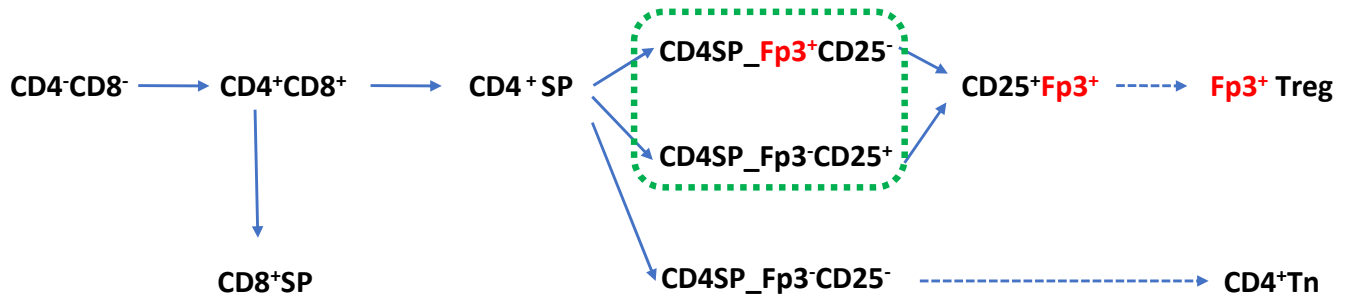
877 50 Alexa A, R. J. topGO: Enrichment Analysis for Gene Ontology. R package version 2.50.0.
878 (2022).

879 51 Zhang, Y. *et al.* Model-based analysis of ChIP-Seq (MACS). *Genome Biol* **9**, R137,
880 doi:10.1186/gb-2008-9-9-r137 (2008).

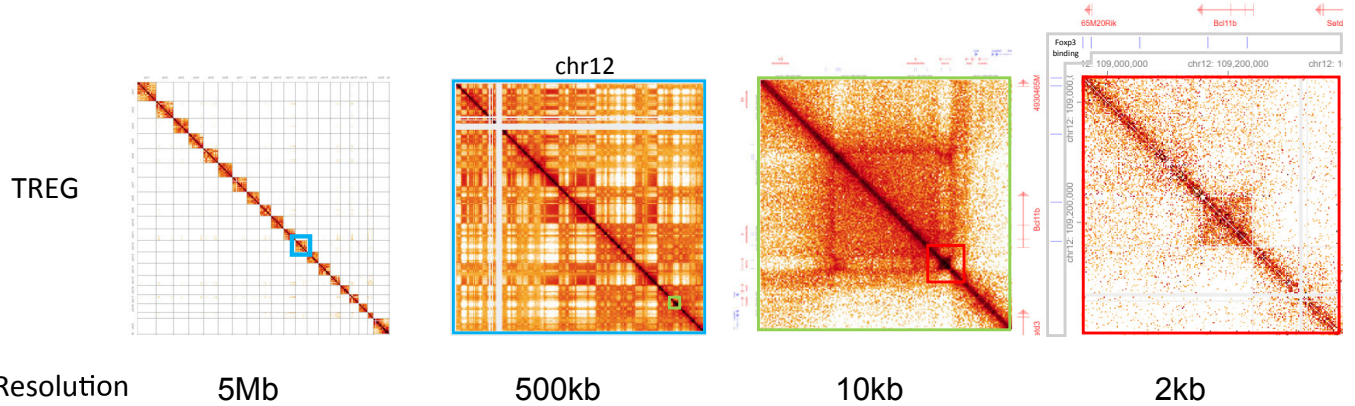
881

882

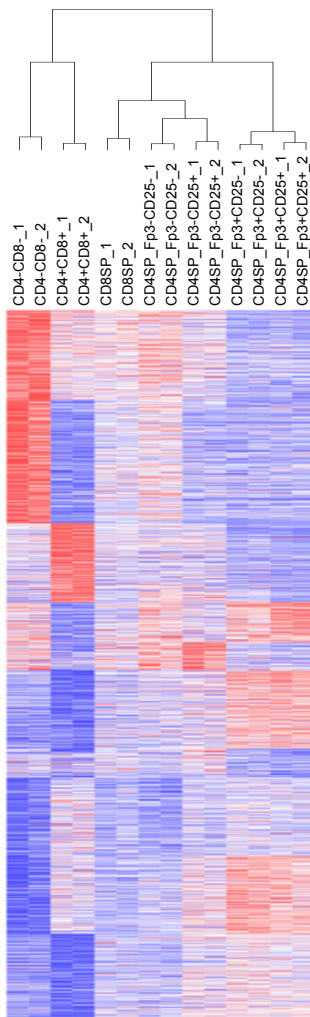
A



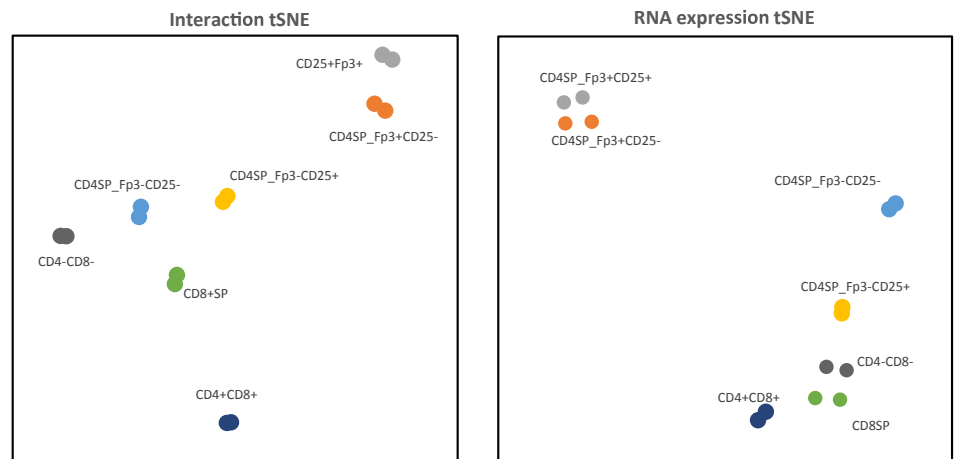
B



C



D



E

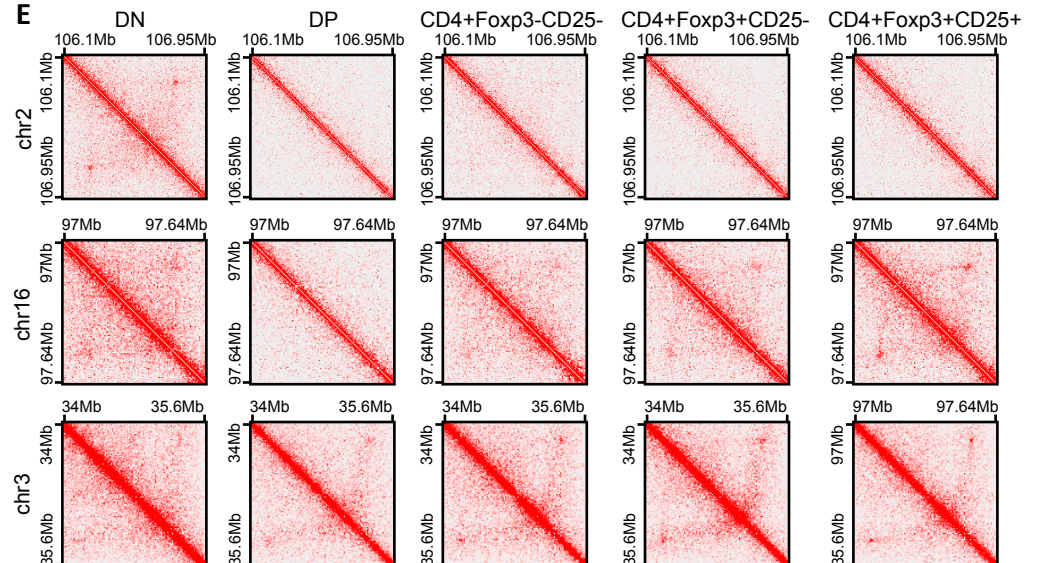


Figure 1

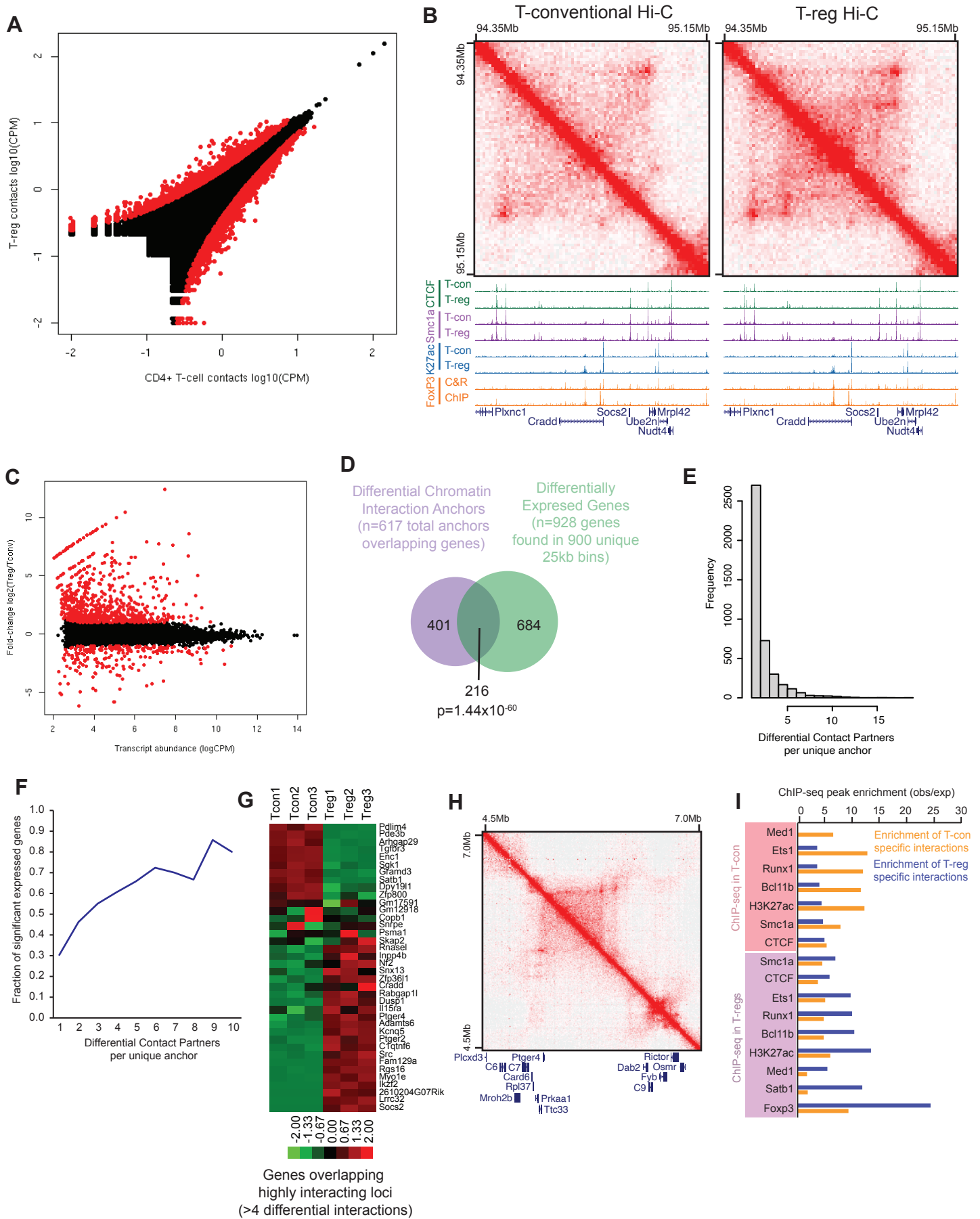


Figure 2

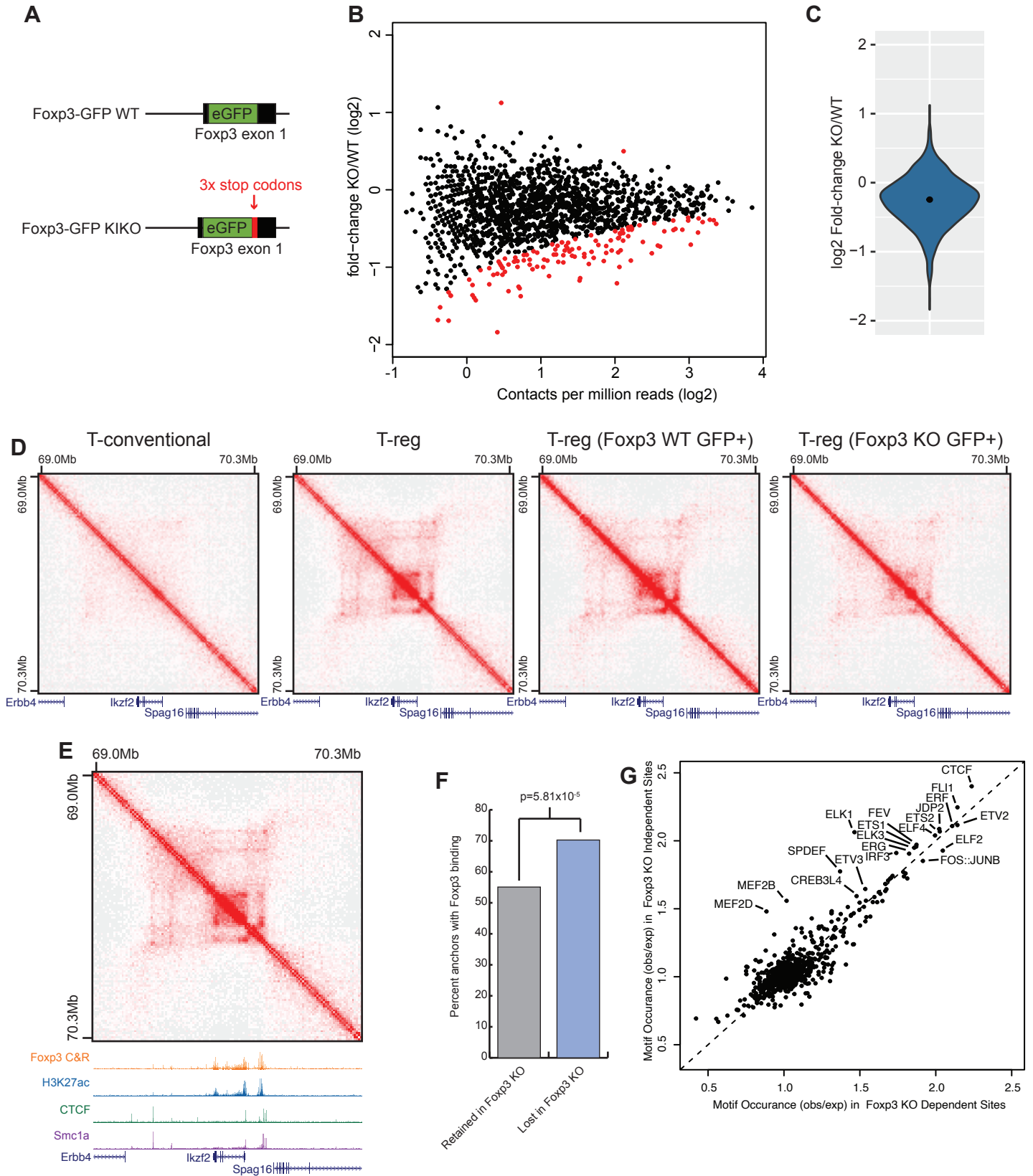


Figure 3

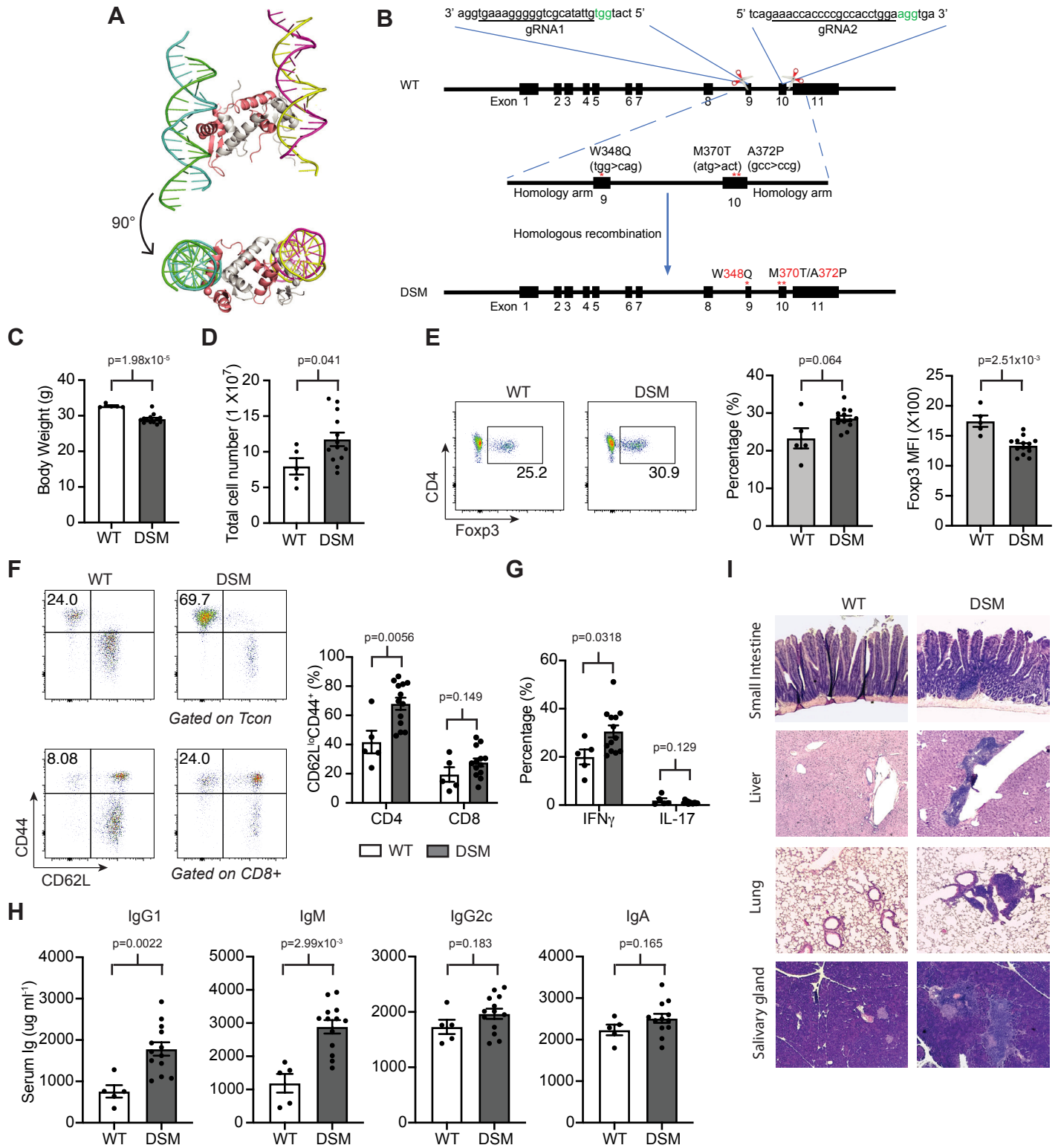


Figure 4

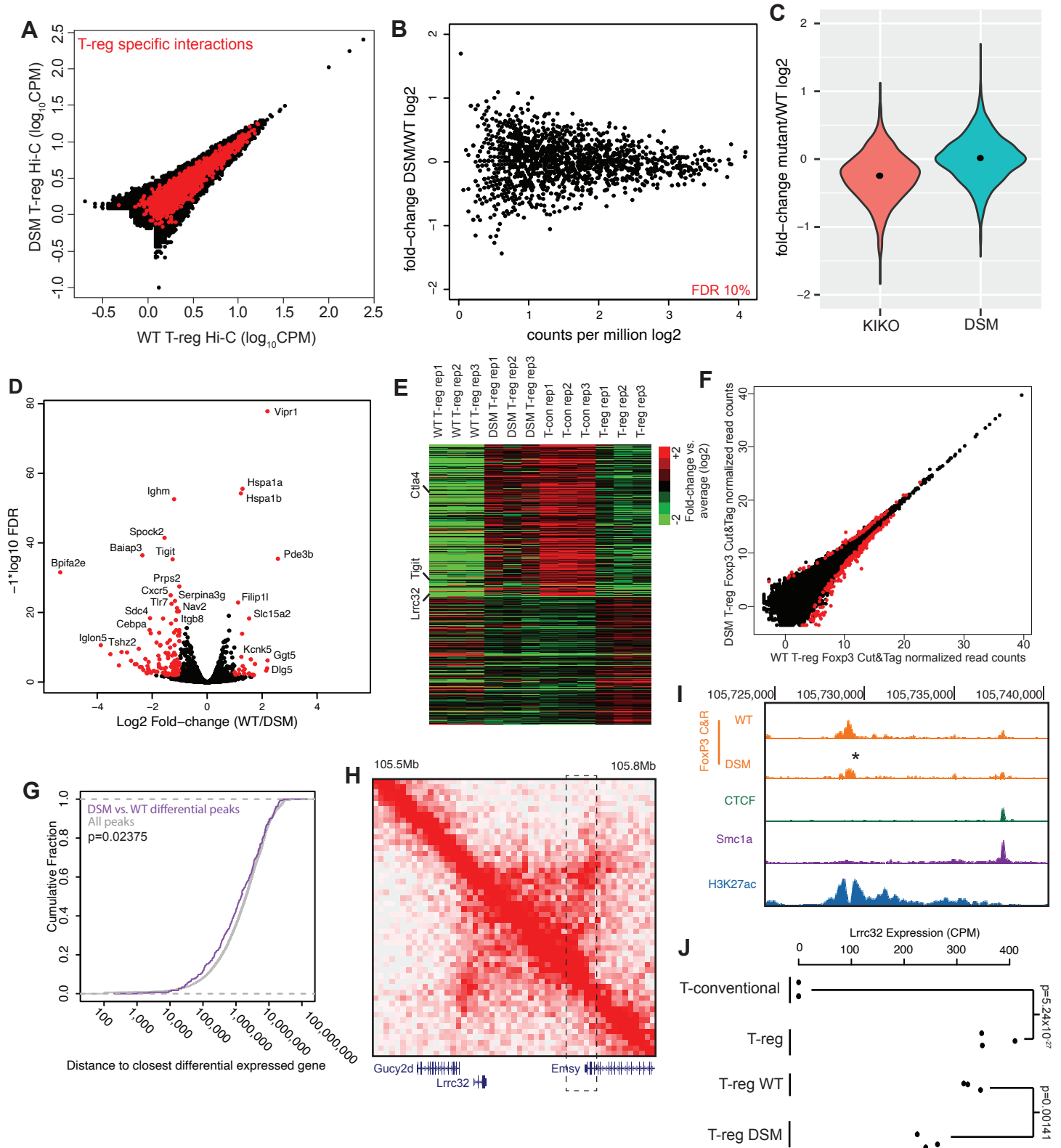


Figure 5

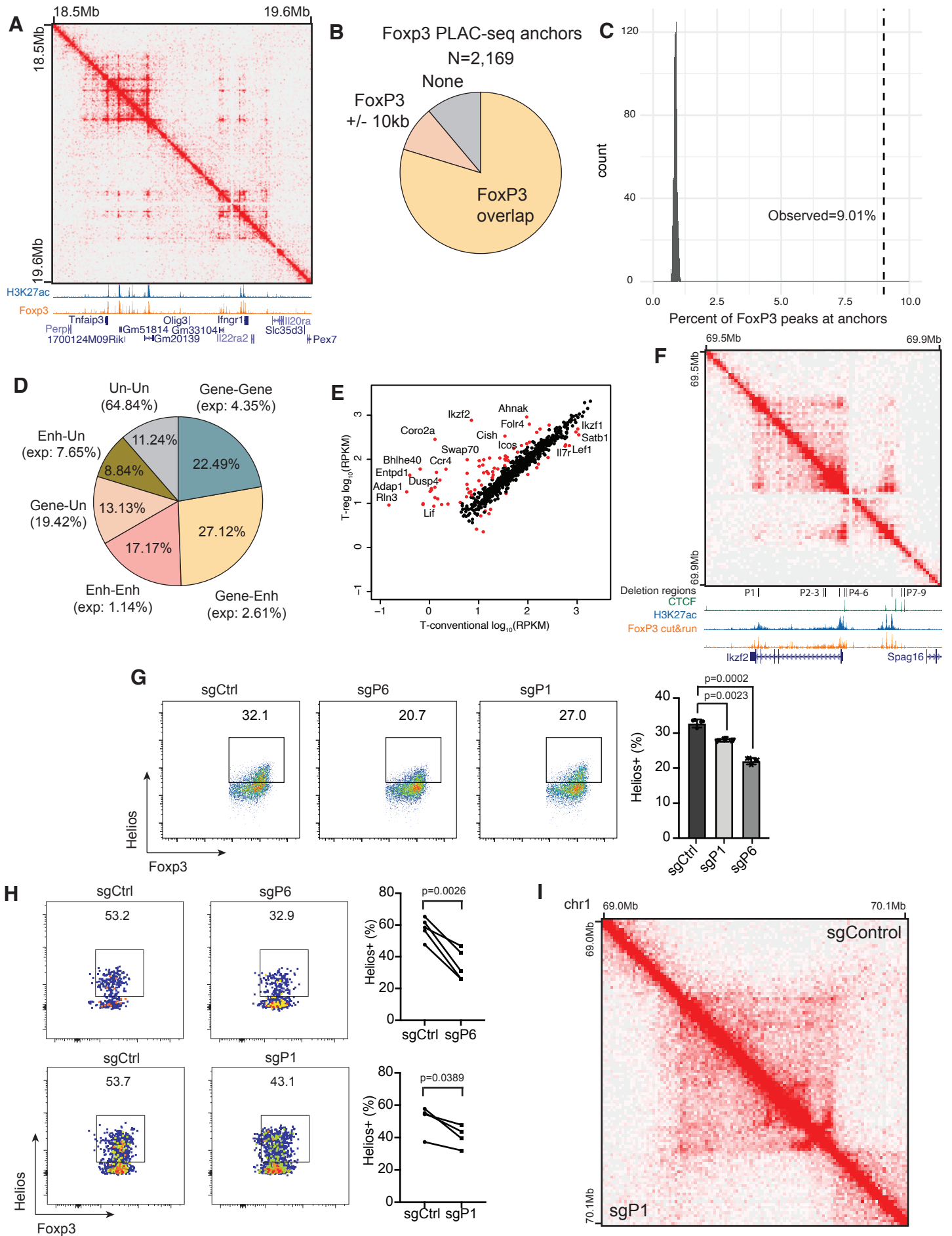


Figure 6

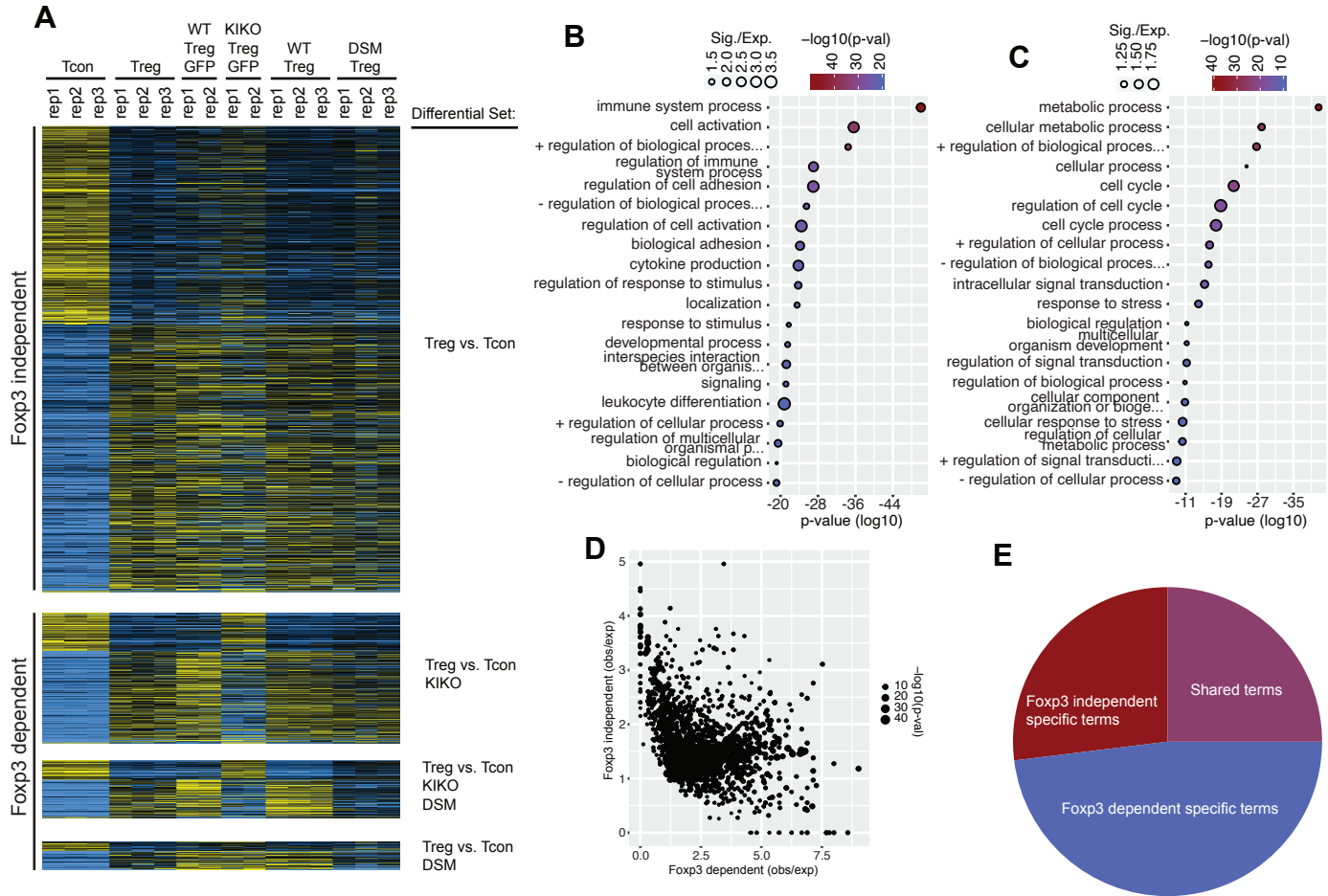


Figure 7